Published in final edited form as:
J Neuropathol Exp Neurol. 2009 July ; 68(7): 785–796. doi:10.1097/NEN.0b013e3181aaf4fd.

Leucine-rich Repeat Kinase 2 Expression Leads to Aggresome Formation that is not Associated with α-Synuclein Inclusions

Elisa A. Waxman, PhD[1], **Jason P. Covy, BS**[1], **Irene Bukh, BS**[1], **Xiaojie Li, MSc**[2,3], **Ted M. Dawson, MD, PhD**[3,4,5], and **Benoit I. Giasson, PhD**[1]

[1]Department of Pharmacology, University of Pennsylvania, Philadelphia, Pennsylvania [2]NeuroRegeneration and Stem Cell Programs, Institute for Cell Engineering, Johns Hopkins University School of Medicine, Baltimore, Maryland [3]Graduate Program in Cellular and Molecular Medicine, Johns Hopkins University School of Medicine, Baltimore, Maryland [4]Department of Neurology, Johns Hopkins University School of Medicine, Baltimore, Maryland [5]Department of Solomon H. Snyder Department of Neuroscience, Johns Hopkins University School of Medicine, Baltimore, Maryland.

Abstract

Mutations in leucine-rich repeat kinase-2 (LRRK2) are the most common known cause of Parkinson disease (PD), but how this protein results in the pathobiology of PD is unknown. Moreover, there is variability in pathology among cases and α-synuclein (α-syn) neuronal inclusions are often present but whether LRRK2 is present in these pathological inclusions is controversial. This study characterizes novel LRRK2 antibodies, some of which preferentially recognize an aggregated form of LRRK2, as observed in cell culture models. Large perinuclear aggregates containing LRRK2 were promoted by proteasome inhibition and prevented by microtubule polymerization inhibition. Further, they were vimentin- and γ-tubulin- but not lamp1-immunoreactive, suggesting that these structures fit the definition of aggresomes. Inhibition of Hsp90 led to degradation of only the soluble/cytosolic pool of LRRK2, suggesting that the aggresomes formed independent of the stability provided by Hsp90. Although these novel anti-LRRK2 antibodies identified aggregates in model cell systems, they did not immunostain pathological inclusions in human brains. Further, co-expression of LRRK2 and α-syn did not recruit α-syn into aggresomes in cultured cells, even in the presence of proteasome inhibition. Thus, although LRRK2 is a model system for aggresome formation, LRRK2 is not present in α-syn pathological inclusions.

Keywords

α-synuclein; Aggregation; Aggresome; Antibody; LRRK2; Parkinson disease

INTRODUCTION

Parkinson disease (PD) is characterized by bradykinesia, resting tremor, cogwheel rigidity and postural instability (1,2) and is associated with the loss of dopaminergic neurons in the substantia nigra pars compacta (3,4). Pathological analysis of PD brains reveals intracytoplasmic, perikaryal inclusions, known as Lewy bodies (LBs) in some of the remaining

Correspondence and reprint requests to: Dr. Benoit I. Giasson, Department of Pharmacology, University of Pennsylvania School of Medicine, 3620 Hamilton Walk, 125 John Morgan, Building, Philadelphia, PA 19104-6084; Tel: 215-573-6012; Fax: 215-573-2236; E-mail: giassonb@mail.med.upenn.edu.

dopaminergic neurons, as well as similar inclusions in neuronal processes, termed Lewy neurites (5–7).

Familial mutations in PD have provided useful insight into the pathobiology of PD. While mutations in *SCNA*, the gene for α-synuclein (α-syn), are relatively rare, studies show a causal relationship between this mutation and disease state such that α-syn is now recognized as the major component of Lewy pathology (5,8,9). Recent discoveries of autosomal dominant missense mutations in *leucine-rich-repeat kinase-2* (*LRRK2; PARK8*) have been identified as the most common genetic cause of sporadic and familial PD cases (10–12). The LRRK2 protein is approximately 280 kDa and contains several complex domains including Ras/GTPase-like (Roc), C-terminal of Roc (COR), kinase (MAPKKK) and WD40 (10–12). Despite its predominance in PD, the function of LRRK2 is currently unknown and the manner by which LRRK2 mutations lead to disease requires further investigation.

Although patients with mutations in LRRK2 exhibit diverse pathological findings, the majority of cases show typical α-syn-positive Lewy pathology (12,13). There is, however, considerable debate as to the presence of LRRK2 in neuronal α-syn pathological inclusions. Some studies report strong LRRK2 immunoreactivity in a subset (10%–15%) of these lesions (14–18), whereas others report only weak staining (19,20) or a complete lack of immunoreactivity (17–19,21,22). Differences in antibody epitopes or lack of antibody specificity have been provided as potential explanations for these variable results (17–19,22).

In the current study, we have designed and characterized novel LRRK2 antibodies for independent investigation of the localization and pathological association of this protein. Using this new set of unique antibodies, we illustrate a lack of association between LRRK2 and α-syn in cultured cells and in Lewy pathology. Additionally, we have characterized large, perinuclear aggregates that are formed by LRRK2 in cultured cells as aggresomes. Our data identify the ability of LRRK2 to form inclusion-like aggregates that do not associate with α-syn.

MATERIALS AND METHODS

Complementary DNA Constructs

The full-length human LRRK2 complementary DNA (cDNA) was amplified with or without a stop codon by PCR using Taq polymerase AccuPrime SuperMix (Invitrogen, Carlsbad, CA) and cloned by topoisomerase reaction into the shuttling vector pCR8/GW/TOPO. To generate the G2019S mutation, the cDNA fragment spanning the AvrII and NcoI restriction sites in LRRK2 was amplified by PCR and cloned by topoisomerase reaction into the vector pCR4-TOPO (Invitrogen). The mutation corresponding to the G2019S amino acid substitution was generated using the QuickChange Site Directed Mutagenesis Kit (Stratagene, La Jolla, CA). The AvrII/NcoI DNA fragments containing the G2019S mutant was reintroduced into full-length LRRK2 by subcloning with these restriction enzymes. The sequence of the plasmids were verified by DNA sequencing using primers that span the whole cDNA as a service offered by the DNA Sequencing Facility of the University of Pennsylvania.

Full-length wild-type (WT) (with or without a stop codon) and G2019S (without a stop codon) LRRK2 cDNAs were introduced into the mammalian expression vector pEF-DEST51 (Invitrogen) by recombinase reaction using LR Clonase II enzyme (Invitrogen) to generate a plasmid expressing full-length LRRK2 without a tag (pEF-DEST51-LRRK2, referred to as LRRK2) or full-length LRRK2 with a C-terminal V5-tagged (pEF-DEST51-LRRK2-V5, referred to as LRRK2-V5).

The cDNA corresponding to amino acids 841 to 960 in human LRRK2 followed by a stop codon was amplified by PCR using Taq polymerase AccuPrime SuperMix (Invitrogen) and cloned by topoisomerase reaction into the shuttling vector pCR8/GW/TOPO. This cDNA was cloned into the bacterial expression vector pDEST17 vector by recombinase reaction using LR Clonase II enzyme (Invitrogen) to generate a plasmid expressing N-terminal His-tagged $LRRK2_{841–960}$ protein. Additional cDNA vectors used include human α-syn in the mammalian-expressing vector pcDNA3.1(23) and pcDNA3.1 (pcDNA) as a vector control.

Expression and Purification of His-Tagged $LRRK2_{841–960}$

BL21 (DE3) *Escherichia coli* were transformed with the pDEST17 $LRRK2_{841–960}$ plasmid and cultured with 100 μg/ml ampicillin. Isopropyl-β-D-thiogalactopyranoside (500 μM) was added for 1.5 hours to induce the expression of His-tagged $Lrrk2_{841–960}$. Bacteria were harvested by sedimentation and resuspended in lysis buffer (25% sucrose, 2 mg/ml lysozyme, 1 mM EDTA, 50 mM Tris, pH 8.0) and incubated on ice for 30 minutes. DNAse I (10 μg/mL), RNAse A (10 μg/mL), 10 mM $MgCl_2$ and 1 mM $MnCl_2$ were added for an additional 30-minute incubation. Two-fold volume of detergent buffer (0.2 M NaCl, 1% deoxycholic acid, 1% NP40, 20 mM Tris, pH 7.5, 2 mM EDTA) was added and the insoluble material containing His-tagged $LRRK2_{841–960}$ was pelleted at 5,000 × *g*. The insoluble fraction was washed with 0.5% Triton, 1 mM EDTA before resuspension in binding buffer (8 M urea, 10 mM Tris, pH 8.0) plus 10 mM imidazole. Insoluble material was cleared at sedimentation at 5,000 × *g*, and the supernatant was incubated with Ni-NTA resin (Novagen, EMD Biosciences, San Diego, CA) for 2 hours at 4°C before clearance on a gravity flow column. Beads were washed multiple times with binding buffer plus 50 mM imidazole before incubation with elution buffer (300 mM imidazole, 8 M Urea, 10 mM Tris, pH 8.0). Eluants were dialyzed against 4 M urea/phosphate-buffered saline (PBS) for 4 to 6 hours at 4°C.

Antibodies

2-2E8 is a novel mouse monoclonal antibody raised against recombinant His-tagged $LRRK2_{841–960}$ purified protein, using previously described methods (24,25). Rabbit polyclonal antibodies 2001 and 2002 were raised against the synthetic HPLC-purified peptide KNENQENDDEGEEDKLC (GenScript Corp., Piscatway, NJ) corresponding to amino acid residues 332–347 in human LRRK2 with a C-terminal Cys and conjugated to maleimide-activated keyhole limpet hemocyanin (Thermo Scientific, Rockford, IL). Rabbit polyclonal antibodies 1181 and 1182 were raised against recombinant His-tagged $LRRK2_{841–960}$ purified protein. All rabbit polyclonal antibodies were generated as a service provided by Covance (Denver, PA). Each rabbit generated 4 bleeds that were identified #1 to #4.

Additional antibodies used were monoclonal anti-V5 (Invitrogen), rabbit polyclonal anti-V5 (Sigma-Aldrich, St. Louis, MO), anti-vimentin (Sigma-Aldrich), anti-lamp1 (BD Biosciences, San Jose, CA), anti-γ-tubulin (Sigma-Aldrich), Syn211 (25), Syn 505 (26), SNL-4 (25), and LB509 (27).

Affinity Purification of Rabbit Polyclonal Antibody to LRRK2

HPLC-purified synthetic peptide B (CQMKSAVEEGTASGSDGNFSEDVLSKFDE) and peptide E (CNSLGPIFDHEDLLKRKRKILSSDDSLR) corresponding to residues 847–874 and 934–960 in LRRK2 with an added N-terminal Cys residue, respectively, were generated as a service by GenScript Corp. The peptides were conjugated to agarose beads using the SulfoLink Immobilization Kit (Thermo Scientific). Polyclonal serum 1182#3 diluted 1:1 in PBS was incubated with the peptide-conjugated agarose beads for 1 hour. Beads were thoroughly washed with PBS and the antibody was eluted with IgG elution buffer (0.2 M glycine, pH 3.0). Neutralization buffer (1 M Tris, pH. 8.5) was added at a 1:20 ratio and the antibody was dialyzed overnight against PBS.

Cell Culture and Transfection

HEK 293 cells stably expressing green fluorescence protein ubiquitin proteasome reporter (GFPu) (28,29) were generously provided by Dr. Randall N. Pittman (University of Pennsylvania); HEK 293t (293t) cells and COS-7 cells were maintained using Dulbecco's Modified Eagle's Medium (Invitrogen) supplemented with 10% fetal bovine serum and 1% penicillin/streptomycin. Stable HEK 293 cells were additionally treated with G418 (Sigma-Aldrich; 300 μg/ml). Cells were plated onto glass coverslips or 6-well plates and transfected at approximately 60% confluency using calcium phosphate precipitation, as previously described (30). Cells were maintained for 48 hours after transfection prior to experimentation unless otherwise specified. Transfection efficiency in 293t cells ranged from 70% to 90%, and in COS-7 cells and stable HEK 293 cells ranged from 10% to 30%.

In some experiments, cultures were treated with the following drugs purchased from Calbiochem (EMD Biosciences) for 12 to 16 hours prior to experimentation: MG132 [Z-Leu-Leu-Leu-al; 10 μM], nocodazole (0.5 μg/ml) and geldanamycin (500 nM). Treatments were matched with a vehicle control of 0.1% DMSO (Fisher Scientific, Fair Lawn, NJ). No differences between untreated and vehicle-treated cells were noted. Total cell lysates were harvested in 1.5X Laemmli sample buffer (75 mM Tris-HCl, pH 6.8, 3% SDS, 15% glycerol, 3.75 mM EDTA, pH 7.4) and boiled. The indicated buffer was used to fully denature protein prior to Western blot analysis. Protein concentration was determined using bicinchoninic acid (BCA) protein assay reagent (Pierce, Fisher Scientific). Western blot analysis was performed on 30 μg of protein for total cell lysates, except as otherwise specified.

Biochemical Cellular Fractionation

Cells were washed once in ice-cold PBS and samples were harvested in 25 mM Tris-HCl, pH 7.5, 150 mM NaCl, 1 mM EDTA, 1% Triton X-100, 20 mM NaF and a cocktail of protease inhibitors containing 1 Mm phenylmethylsulfonyl and 1 mg/ml each of pepstatin, leupeptin, N-tosyl-L-phenylalanyl chloromethyl ketone, N-tosyl-lysine chloromethyl ketone and soybean trypsin inhibitor. Samples were sedimented at 100,000 × *g* for 30 minutes at 4°C. Supernatants were removed and pellets were sonicated in 1.5X Laemmli sample buffer. SDS sample buffer was added and samples were heated to 100°C for 5 minutes prior to Western blot analysis. Equal proportions of supernatant and pellet were loaded and analyzed as percent pelleted.

Western Blot Analysis

Protein samples were resolved by SDS-PAGE followed by electrophoresis onto nitrocellulose membranes. Membranes were blocked in Tris-buffered saline (TBS) with 5% dry milk and incubated overnight with the LRRK2-specific antibodies described above, anti-V5, or -Syn211 (α-syn) in TBS/5% dry milk. Each incubation was followed by goat anti-mouse conjugated horseradish peroxidase (HRP) (Amersham Biosciences, Piscataway, NJ) or goat anti-rabbit HRP (Cell Signaling Technology, Danvers, MA) and immunoreactivity was detected using chemiluminescent reagent (NEN, Boston, MA) followed by exposure on X-ray film.

Cell Culture Immunofluorescence

Immunofluorescence of transfected cells was performed as previously described (31). Cells were fixed at −20°C with 100% methanol for 20 minutes followed by 50% methanol and 50% acetone for 5 minutes. Following washes with PBS, coverslips were blocked with PBS containing 5% bovine serum albumin and primary antibodies were diluted into blocking solution for 1 to 2 hours at room temperature. Antibodies were used at the following concentrations: polyclonal anti-LRRK2 antibodies (1:1000), monoclonal anti-LRRK2 antibody (1:100), affinity purified anti-LRRK2 antibodies (1:500), monoclonal anti-V5 (1:2000), polyclonal anti-V5 (1:1000), anti-vimentin (1:250), anti-lamp1 (1:250), anti-γ-

tubulin (1:1000), and Syn211 (1:2000). After PBS washes, coverslips were incubated with goat anti-mouse secondary conjugated to Alexa 594 and goat anti-rabbit secondary conjugated to Alexa 488. Nuclei were counterstained with Hoechst trihydrochloride trihydrate 33342 (Invitrogen), and coverslips were mounted using Cytoseal 60 (Fisher Scientific).

Fluorescence Microscopy

Immunofluorescence was captured on an Olympus BX51 fluorescence microscope mounted with a DP71 digital camera. Cellular colocalization images were captured on a Zeiss Axiovert 200M inverted confocal microscope mounted with a Zeiss LSM510 META NLO digital camera utilizing Zeiss LSM510 META V3.2 confocal microscope software. Confocal images were captured with 63x oil optics and all representative images were of one Z-plane of <0.7 μm.

Immunohistochemistry

Postmortem brain samples from patients with PD, neurodegeneration with brain iron accumulation 1, Lewy body variant of Alzheimer disease, dementia with Lewy bodies, or multiple systems atrophy were harvested, fixed and processed as previously described (32, 33). Sequential 6-μm tissue sections were immunostained using the avidin-biotin complex detection system (Vector Laboratories, Burlingame, CA) and 3,3'-diaminobenzidine. For some sections, pretreatment with 70% formic acid was used to enhance antigen detection. Primary antibodies were incubated overnight in Tris with 5% fetal bovine serum (FBS). Tissue sections were lightly counterstained with hematoxylin. Co-occurrence of LBs and glial cytoplasmic inclusions were assessed by independent assessment of adjacent sections.

Immunofluorescence of Postmortem Samples

Immunofluorescence was completed with paraffin-embedded brain sections as previously described (33). Sections were incubated overnight with primary antibodies, diluted in Tris/ 5% dry milk or in Tris/ 5% FBS, followed by goat anti-mouse secondary conjugated to Alexa 594 and goat anti-rabbit secondary conjugated to Alexa 488 (Invitrogen, Carlsbad, CA). Anti-LRRK2 antibodies were used at the same concentrations that were effective by Western blot analysis: 1:1000 for polyclonal antibodies, 1:100 for monoclonal 2-2E8, and 1:100 for affinity purified antibodies. Nuclei were counterstained with 4',6-diamidino-2-phenylindole, and sections were post-fixed with formalin and coverslipped using Cytoseal 60 (Fisher Scientific).

Analysis of Wild-Type and Knockout Mouse Samples

Mouse brain tissue from a 10-week-old female mouse was homogenized in 4X volumes of ice-cold PBS containing 0.1% Triton X-100 with protease inhibitors (0.5 mM AEBSF (Sigma), 2 μg/ml Aprotinin (Roche), 5 μg/ml Bestatin (Sigma), 5 μg/ml E-64 (Roche), 5 μg/ml Leupeptin (Roche), and 1 μg/ml Pepstatin (Sigma)). The tissue homogenate was centrifuged at 37,000 × *g* at 4°C for 20 minutes. The supernatant was removed and protein concentration measured by BCA protein assay. For Western blot analysis, 40 μg mouse brain protein extracts were resolved by SDS-PAGE gel, and electrophoresed onto nitrocellulose membranes. After transfer, the membranes were blocked with 5% non-fat milk, and incubated with primary anti-LRRK2 antibody overnight at 4°C using 1:100 dilution or actin (Sigma) at 1:10,000 dilution. After extensive washing with TBS + 0.1% Tween buffer, the blot was incubated with anti-rabbit-HRP antibody (GE Healthcare, Piscataway, NJ) at room temperature for 1 hour. Western signal was detected by SuperSignal West Pico Chemiluminescent Substrate (Thermo Scientific). LRRK2 knockout mice were generated by disruption of exon 40 of the LRRK2 gene (S. Biskup, M. Sasaki, T.M. Dawson and V.L. Dawson, unpublished data). LRRK2 knockout mice have been outbred and maintained on a C57BL/6J background.

Quantitative Analysis

Western blot data was quantified by ImageJ software (NIH). Data were analyzed as a change of percent pelleted from vehicle control conditions. Cells were counted in a blinded fashion, and percentage was determined by averaging 2 to 3 fields per independent experiment. All comparisons were completed by 2-way, parametric t-tests using GraphPad InStat software (GraphPad, San Diego, CA).

RESULTS

Characterization of Novel Anti-LRRK2 Antibodies

Our laboratory generated a new series of LRRK2-specific antibodies directed towards either amino acids 841–960 (antibodies termed 1181, 1182, and 2-2E8) or amino acids 332–347 (antibodies termed 2001 and 2002) of human LRRK2. 2-2E8 is a mouse monoclonal antibody; the others are rabbit polyclonal antibodies. To verify the specificity of these antibodies, 293t cells were transfected with C-terminal V5 tagged LRRK2 (LRRK2-V5) or untagged LRRK2 and cell lysates were harvested 48 hours after transfection for Western blot analysis. The immunoreactivity of each antibody was compared against a mock-transfection control (pcDNA) for specificity (Fig. 1). All antibodies tested specifically recognized both V5-tagged and untagged LRRK2 with little variability noted between different bleeds of 1181 and 1182 rabbit polyclonal antibodies (data not shown). Due to differing specificity between bleeds of antibodies 2001 and 2002 (data not shown), 2001#1 and 2002#2 were chosen for Western blot analyses (Fig. 1E, F) and further studies. Although all antibodies specifically recognized full-length LRRK2 (at ~280 kDa), V5, 1181, 1182, and 2-2E8 additionally recognized a specific breakdown product of ~240 kDa. This was not recognized by the 2001 and 2002 antibodies, suggesting N-terminal proteolysis after amino acid 347.

Antibodies were then tested in 293t cells transfected with LRRK2-V5 by double immunofluorescence against anti-V5 antibodies. Different bleeds of 1181 and 1182 were compared. Antibody 1181#1 preferentially reacted with perinuclear aggregates of LRRK2, compared to the staining pattern of an anti-V5 antibody that recognized both general cytoplasmic and aggregated LRRK2 (Fig. 2A); however, 1181#2 (and subsequent bleeds) showed increased immunoreactivity of both aggregate and cytosolic LRRK2 (Fig. 2B). Similar specificity patterns were observed between bleed #1 and #2 for antisera 1182 (Fig. 2C, D). Mouse monoclonal antibody 2-2E8 specifically detected the aggregated form of LRRK2. Antibody 2001#1 also identified, albeit weakly, aggregated LRRK2; antibody 2002#2 did not show specific immunoreactivity by immunofluorescence (data not shown). The selectivity of antibody 2-2E8 and the early bleeds of serum 1181 and 1182 for aggregates of LRRK2 may be due at least in part to having used bacterially expressed detergent insoluble fractions of $LRRK2_{841–960}$ as the antigen. The same staining pattern and specificity for aggregates were observed when cells were transfected with untagged LRRK2 or LRRK2 with the G2019S mutation (data not shown). No difference in prevalence or morphology between the WT and the G2019S mutation was observed.

Characterization of LRRK2 Aggregates

Previous studies have identified aggregated LRRK2 in a subset of cultured cells (14,34); however, none were as prevalent as observed in 293t cells with an antibody directed at the 841–960 region of LRRK2. The percentages of cells containing aggregates varied with transfection efficiency (data not shown) but aggregates were readily observed 48 hours post-transfection; this was the time point chosen for subsequent examination. Since LRRK2 can be degraded through the proteasome (35,36), we blocked proteasome function with MG132 to identify any alterations in aggregate formation (Fig. 3A–C). Treatment with MG132 approximately doubled the percentage of cells that exhibited aggregates.

The microtubule polymerization inhibitor nocodazole alters microtubule-dependent cellular activity and activates Raf1 and MAPK pathways (37). Previous studies report that LRRK2 aggregation is prevented with nocodazole treatment (14). Nocodazole added 12 hours after transfection blocked the formation of large perinuclear aggregates that were first observed at 24 hours post-transfection (Fig. 3D, E). Antibody 1181#1, however, identified smaller punctate staining of aggregates in the cytosol, suggesting that microtubule transport or another downstream pathway altered by nocodazole is required for the formation of large perinuclear aggregates but not for general aggregation of LRRK2 in small complexes.

Because LRRK2 can form aggregates in a subset of cells that are not challenged by exogenous proteasome inhibitors, we hypothesized that LRRK2 may create a proteasome deficit in transfected cells. We used HEK 293 cells stably transfected with GFP-u, a short-lived GFP construct, which is readily degraded by the proteasome but accumulates when the proteasome is inhibited (28,29). These cells were transfected with LRRK2-V5 and double immunofluorescence was performed between V5 and GFP. No increase in GFP fluorescence was observed regardless of LRRK2 aggregation (Fig. 4A, arrow); however, MG132 treatment resulted in increased GFP fluorescence with occasional GFP colocalization with LRRK2 aggregates (Fig. 4B, arrowhead).

To confirm that LRRK2 aggregation is not cell type-dependent, we investigated the ability of our antibodies to detect similar inclusions in COS-7 cells, as reported by Greggio and colleagues (14). Large LRRK2 aggregates were observed in these cells albeit at a lower frequency (Fig. 5A; 5% ± 3% [SD] under basal conditions). Similar to 293t cells, aggregate formation was promoted by MG132 to 72% ± 13% [SD] ($p < 0.0001$, $n = 4$); the formation of large perinuclear aggregates was also blocked with concomitant treatment with nocodazole (Fig. 5B, C).

LRRK2 Inclusions Have Properties Similar to Aggresomes

Cellular mechanisms often attempt to sequester misfolded proteins into perinuclear aggregates called “aggresomes.” Overexpression of particular proteins or proteasome inhibition can promote aggresome formation which can be blocked with nocodazole treatment (38). The ability of LRRK2 to form aggresome-like structures was further investigated using confocal microscopy with cellular markers that colocalize with aggresomes (i.e. vimentin and γ-tubulin) and with lamp1, which often surrounds aggresomes (38–40).

293t and COS-7 cells were transfected with untagged LRRK2 and immunostained with antibody 1181#1 and either anti-vimentin, anti-γ-tubulin, or anti-lamp1. MG-132 was used to enhance LRRK2 aggregation in COS-7 cells. In both 293t (Fig. 6A–C) and COS-7 cells (Fig. 6D–F), large LRRK2 aggregates colocalized with vimentin and γ-tubulin. Lamp1 immunofluorescence appeared throughout the cytosol with some immunoreactivity around the large perinuclear aggregates (Fig. 6C, F), consistent with the typical staining pattern of aggresomes (38–40). These results were replicated with V5 tagged LRRK2 (data not shown).

Formation of LRRK2 Aggresomes Is Independent of Hsp90

Proteasomal degradation of LRRK2 is promoted through inhibition of heat shock protein 90 (Hsp90) (35,41). We therefore examined the effects of the Hsp90 inhibitor geldanamycin on LRRK2 aggresome formation in 293t cells. At 32 hours post-transfection, cells were treated with geldanamycin for an additional 16 hours post-transfection. No difference in LRRK2 aggresome formation was observed by immunofluorescence (data not shown). Since aggresome formation can also be monitored biochemically (38), cells were biochemically fractionated and analyzed by Western blot analysis to identify subtle changes in LRRK2 expression and distribution. LRRK2 was fractionated to separate the soluble cytosolic portion

(supernatant) of LRRK2 from the insoluble aggregated form (pellet). Comparable to the characterization of LRRK2 observed by immunofluorescence, MG-132 treatment redistributed LRRK2 towards the insoluble aggregated form of the protein (Fig. 7A). Geldanamycin treatment did not alter the amount of LRRK2 in the pellet, but it significantly decreased the amount of LRRK2 in the soluble fraction ($p = 0.04$, $n = 3$), consistent with a role for Hsp90 in stabilizing the soluble pool of LRRK2. Concomitant treatment of MG132 and geldanamycin increased the amount of LRRK2 in the pellet fraction and decreased the amount of LRRK2 in the soluble fraction when compared to geldanamycin treatment alone. The effects of concomitant treatment with MG132 and geldanamycin were similar to challenge with MG132 alone.

Since Hsp90 may only stabilize newly generated protein, rather than mature protein, we aimed to examine the role of Hsp90 on early aggresome formation by minimizing protein production prior to treatment. 293t cells were treated with geldanamycin shortly (12 hours) after transfection and then biochemically fractionated at 24 hours. This experimental paradigm yielded similar results, i.e. geldanamycin treatment reduced the amount of soluble LRRK2 but it did not prevent aggresome formation (Fig. 7B). Complete redistribution of LRRK2 into the pellet was observed with MG132 treatment either with or without geldanamycin co-treatment. These results suggest that Hsp90 activity is only involved with the soluble pool of LRRK2 and that without Hsp90 activity this pool of LRRK2 is degraded by the proteasome. Under conditions of proteasomal inhibition, however, this pool of LRRK2 is also recruited into the aggresome.

Immunohistochemical Analyses of α-Syn Inclusions in Brain with LRRK2 Antibodies

We next examined the immunoreactivity of the anti-LRRK2 antibodies for α-syn-positive pathological inclusions in brain sections from patients diagnosed with PD and other α-synucleinopathies (Table). Antibodies 1181#1 and #2, 1182#1 and #2, 2001#1, 2002#2 and 2-2E8 were used to immunostain paraffin-embedded tissue sections, and adjacent sections were stained with the anti-α-syn antibody LB509. LRRK2 immunoreactivity was absent in α-syn pathological inclusions by immunocytochemistry (data not shown). Double immunofluorescence was also performed with 1181#1, 1182#1, 2-2E8, 2001#1, and 2002#2 and the α-syn-specific antibodies Syn505, LB509, or SNL4. Similarly, there was an overall paucity of LRRK2 immunoreactivity for α-syn pathological inclusions (Fig. 8). Faint LRRK2 staining colocalizing with α-syn immunoreactivity was noted in some rare LBs (Fig. 8A, arrow) but this immunoreactivity was equivalent to that of other low-level staining in each sample; LRRK2 immunoreactivity did not colocalize with any α-syn-positive neurites. These findings indicate that LRRK2 does not accumulate in α-syn pathological inclusions.

To further verify the specificity of our antibodies, we affinity purified antibody 1182 with several separate peptides, and the antibodies (termed 1182B and 1182E, respectively) purified with peptides B and E were selected for their specificity and strong immunoreactivity (Fig. 9A). A specific band at ~280 kDa was identified for both of these affinity purified antibodies in transfected 293t cells (+), but not untransfected cells (−). Further, specific immunoreactivity of endogenous LRRK2 protein was identified in mouse brain and in 4 samples of human cerebral cortices (H1-4). In samples H1 and H4, a postmortem degradation product of approximately 150 kDa consistent with the degradation product previously identified with antibody AP7099b (21) was prominently observed. The specificities of antibodies 1181B and 1181E were further examined on samples from WT and LRRK2 knockout mice (Fig. 9B). These antibodies recognized specific immunoreactivity at ~280 kDa only in the WT mouse sample. Minimal non-specific cross-reactivity was observed.

Specificity of these antibodies was further assessed by double immunofluorescence on 293t cells transfected with LRRK2-V5. 1182B (data not shown) and 1182E (Fig. 9C) exhibited

complete overlay with anti-V5 immunoreactivity, identifying both soluble and aggregated (arrowheads) LRRK2 in transfected cells. Although 1182B and 1182E did not preferentially recognize the aggregated form of LRRK2, these antibodies did show specific immunoreactivity.

Immunohistochemical analyses were performed with 1182B and 1182E on paraffin-embedded tissue sections and adjacent sections were stained with the anti-α-syn antibody LB509. α-Syn inclusions were negative for LRRK2 immunoreactivity (data not shown). Double immunofluorescence was also performed with these affinity purified anti-LRRK2 antibodies and anti-α-syn mouse monoclonal antibody Syn505 (Fig. 9D, E). LRRK2 immunoreactivity did not colocalize with α-syn-positive pathological inclusions.

Lack of Interaction Between LRRK2-Aggresomes and α-Syn in Cultured Cells

Some studies have suggested that α-syn can form aggregates similar to aggresomes under certain conditions (42,43), and aggresomes can recruit other proteins, including α-syn in some cases (39,40,44). 293t cells were co-transfected with α-syn and LRRK2-V5 to determine whether LRRK2 could recruit α-syn into its aggresomes. Co-transfection of α-syn with LRRK2 resulted in fewer aggresomes under basal conditions due to reduced expression of LRRK2 (data not shown). After MG132 treatment aggresomes were observed, albeit at reduced efficiency, compared to transfection with LRRK2 alone (data not shown). In cells that contained LRRK2 aggresomes, α-syn was found by confocal microscopy to remain cytosolic (Fig. 10A). Similarly, biochemical cellular fractionation did not reveal insoluble α-syn with LRRK2 co-expression even after MG132 treatment (Fig. 10B).

DISCUSSION

Aggresome formation is a general cellular process that occurs when proteasomal capacity is exceeded; it can also be an attempt to sequester misfolded proteins (38). Expression of LRRK2 in 293t cells resulted in the spontaneous formation of large perinuclear aggregates that fit the definition of aggresomes as characterized by 1) increased frequency by proteasomal inhibition, 2) colocalization and redistribution of vimentin and γ-tubulin, and 3) the ability to block the formation of these large aggregates with nocodazole, an inhibitor of microtubule polymerization. Further, the LRRK2 aggresomes were shown to be distinct from lysosomes, as indicated by the paucity of lamp1 immunoreactivity for aggregates. Similar findings were found in COS-7 cells, consistent with the previous studies (14), although the basal frequency of these aggresomes were less than in 293t cells.

The presence of LRRK2-induced aggresomes did not appear to have major adverse affects on the cells. Cell toxicity was not observed in 293t or COS-7 cells that expressed LRRK2, either with or without aggresome formation. Nuclei also appeared normal, with the exception of nuclear envelope distortion by larger aggresomes; and aggresome-containing cells were stable through 5 days after transfection (data not shown). This is consistent with other findings that aggresomes may alter the nuclear envelope but may not be toxic (39,40,44).

While LRRK2 aggresome formation was facilitated by proteasome inhibition, LRRK2 expression did not result in aggresome formation due to direct inhibition of proteasome function (Fig. 4). Further, Hsp90, a known component of LRRK2 stability, did not control aggresome formation. Expression of LRRK2 results in 2 pools of proteins. There is a soluble pool of LRRK2 that requires functional Hsp90 for stable folding and would otherwise (i.e. with Hsp90 inhibition) be degraded by the proteasome (35). The second pool of LRRK2 is likely natively misfolded and spontaneously coalesces to form aggregates; the formation of these aggregates is not dependent on Hsp90 activity. This aggregated protein is likely actively transported via microtubules to form aggresomes. Our data suggest that while “normally”

folded protein can be recruited into aggresomes during proteasome dysfunction, the redistribution of this pool of LRRK2 to aggresomes is independent of the protein stability provided by Hsp90. In addition, while Hsp90 inhibition would then promote degradation of soluble LRRK2, concomitant treatment with proteasome inhibitors shuttles all LRRK2 protein into the aggresome, similar to treatment with proteasome inhibitors alone. Although pharmacological inhibition of the proteasome increases the number of aggresomes formed, they may form by a different mechanism than those under unchallenged conditions. The mechanisms that results in LRRK2 aggresome formation may be investigated in future studies.

The current study also characterizes novel LRRK2-specific antibodies directed towards the N-terminal end, some of which like 2-2E8, 1181#1 and 1182#1 preferentially recognize aggregated forms of LRRK2. Further, the affinity purification of serum 1182 resulted in highly specific LRRK2 antibodies (1182B and 1182E) that were clearly capable of specifically detecting endogenous LRRK2 in mouse and human brains. Taking advantage of these tools, we aimed to clarify the controversy surrounding the presence of LRRK2 in LBs and other α-syn-containing pathological inclusions. Using these antibodies we were not able to identify accumulations of LRRK2 in α-syn pathological inclusions by immunohistochemistry or double immunofluorescence microscopy in the brains of patients with diverse α-synucleinopathies, including those with LRRK2 mutations. In some cases, these LRRK2-specific antibodies exhibited faint immunofluorescence in the area of LBs but this immunoreactivity did not identify the halo-structure or core LB profiles noted in some studies (14,16–20). The morphology was more similar to the LRRK2-positive cell bodies reported by others (16,19). Furthermore, affinity-purified antibodies 1182B and 1182E that unequivocally specifically detected endogenous LRRK2 did not label any α-syn pathological inclusions.

Anti-LRRK2 antibodies NB300-268 and NB300-267 are the reagents used in most studies in which a subset of LBs was intensely anti-LRRK2 immunoreactive (14–20). While our previous work also indicates that a small subset of LBs and spheroids can be detected with these antibodies by immunohistochemistry under similar conditions as used in the current study (22), they appear to cross-react to several proteins by Western blot analysis (15,19,22,45,46). Therefore, their positive immunoreactivities to α-syn inclusions are likely due to non-specificity; this is further supported by the inability of other LRRK2 antibodies to recognize α-syn pathological inclusions (17–19).

Differences in antibody epitopes have been suggested as a reason for the paucity of immunostaining of α-syn pathological inclusions with some LRRK2 antibodies (17,18). Antibodies 1181, 1182 and 2-2E8 have epitopes (residues 841–960 in LRRK2) in the same region as the previously used antibody NB300-267 (directed against amino acids 900–1000), providing support against this hypothesis. Even using antigen retrieval, our anti-LRRK2 antibodies that preferentially detect the aggregated forms of LRRK2 and the very specific affinity-purified LRRK2 antibodies were unable to support the presence of LRRK2 in α-syn pathological inclusions.

Consistent with a lack of association between LRRK2 and α-syn, the formation of LRRK2 aggregates in cultured cells that were co-transfected with LRRK2 and α-syn did not result in recruitment of α-syn into these aggresomes. While our studies cannot completely rule out an association between soluble LRRK2 and α-syn, our findings are in agreement with other in vivo studies that indicate a lack of interaction between these 2 proteins (47).

Taken together, the results indicate that LRRK2 can readily form aggresomes when it is over-expressed or when proteasome function is impaired, but that these LRRK2 accumulations do not initiate or promote α-syn inclusion formation. Further, we did not identify a difference in aggresome formation between WT and the G2019S LRRK2, suggesting that the most common

LRRK2 pathological mutation does not potentiate its aggregation. Immunocytochemical studies with the novel LRRK2 antibodies support the contention that LRRK2 is not an important component of α-syn pathological inclusions. Furthermore, since most, but not all patients with the same LRRK2 mutations have neuronal α-syn pathological inclusions, it is unlikely that LRRK2 directly causes the aggregation of α-syn. Mutations in LRRK2 likely alter its enzymatic function, thereby having effects on cellular pathways that result in the formation of α-syn inclusions. Further studies are needed to provide insights into the mechanisms by which LRRK2 mutation results in PD and α-syn pathology.

ACKNOWLEDGMENTS

We thank Drs. Valina L. Dawson, Yulan Xiong, SanXia Wang and Byoung Dae Lee (Johns Hopkins University School of Medicine, Baltimore, MD) for their assistance with the animal husbandry for the LRRK2 knockout mice and immunoblot analysis of these mice. We also thank Drs. John Q. Trojanowski and Virginia M.-Y. Lee (Center for Neurodegenerative Disease Research, University of Pennsylvania) and the families of patients who make this research possible.

This work was funded by grants from the National Institute on Aging (AG09215), the National Institute of Neurological Disorders and Stroke (NS053488 and NS38377) and The Ellison Medical Foundation. E.A.W. was supported by a training grant (T32 AG00255) from the National Institute on Aging. The Biomedical Imaging Core Lab is supported by Abramson Cancer Institute at University of Pennsylvania.

REFERENCES

1. Simuni T, Hurtig HI. Parkinson's disease: The clinical picture. 2000:193–203.
2. Gelb DJ, Oliver E, Gilman S. Diagnostic criteria for Parkinson disease. Arch Neurol 1999;56:33–39. [PubMed: 9923759]
3. Pakkenberg B, Moller A, Gundersen HJ, et al. The absolute number of nerve cells in substantia nigra in normal subjects and in patients with Parkinson's disease estimated with an unbiased stereological method. J Neurol Neurosurg Psychiatry 1991;54:30–33. [PubMed: 2010756]
4. Damier P, Hirsch EC, Agid Y, et al. The substantia nigra of the human brain. II. Patterns of loss of dopamine-containing neurons in Parkinson's disease. Brain 1999;122(Pt 8):1437–1448. [PubMed: 10430830]
5. Goedert M. Alpha-synuclein and neurodegenerative diseases. Nat Rev Neurosci 2001;2:492–501. [PubMed: 11433374]
6. von Bohlen Und HO. Synucleins and their relationship to Parkinson's disease. Cell Tissue Res 2004;318:163–174. [PubMed: 15503152]
7. Lee VM, Trojanowski JQ. Mechanisms of Parkinson's disease linked to pathological alpha-synuclein: new targets for drug discovery. Neuron 2006;52:33–38. [PubMed: 17015225]
8. Forman MS, Lee VM, Trojanowski JQ. Nosology of Parkinson's disease: Looking for the way out of a quagmire. Neuron 2005;47:479–482. [PubMed: 16102530]
9. Spillantini MG, Schmidt ML, Lee VMY, et al. Alpha-synuclein in Lewy bodies. Nature 1997;388:839–840. [PubMed: 9278044]
10. Paisan-Ruiz C, Jain S, Evans EW, et al. Cloning of the gene containing mutations that cause PARK8-linked Parkinson's disease. Neuron 2004;44:595–600. [PubMed: 15541308]
11. Zimprich A, Biskup S, Leitner P, et al. Mutations in LRRK2 cause autosomal-dominant parkinsonism with pleomorphic pathology. Neuron 2004;44:601–607. [PubMed: 15541309]
12. Giasson BI, Van Deerlin VM. Mutations in LRRK2 as a cause of Parkinson's disease. Neurosignals 2008;16:99–105. [PubMed: 18097165]
13. Hasegawa K, Stoessl AJ, Yokoyama T, et al. Familial parkinsonism: Study of original Sagamihara PARK8 (I2020T) kindred with variable clinicopathologic outcomes. Parkinsonism Relat Disord. 2008[Epub ahead of print]
14. Greggio E, Jain S, Kingsbury A, et al. Kinase activity is required for the toxic effects of mutant LRRK2/dardarin. Neurobiol Dis 2006;23:329–341. [PubMed: 16750377]

15. Miklossy J, Arai T, Guo JP, et al. LRRK2 expression in normal and pathologic human brain and in human cell lines. J Neuropathol Exp Neurol 2006;65:953–963. [PubMed: 17021400]

16. Alegre-Abarrategui J, Ansorge O, Esiri M, et al. LRRK2 is a component of granular alpha-synuclein pathology in the brainstem of Parkinson's disease. Neuropathol Appl Neurobiol 2008;34:272–283. [PubMed: 17971075]

17. Zhu X, Babar A, Siedlak SL, et al. LRRK2 in Parkinson's disease and dementia with Lewy bodies. Mol Neurodegener 2006;1:17. [PubMed: 17137507]

18. Zhu X, Siedlak SL, Smith MA, et al. LRRK2 protein is a component of Lewy bodies. Ann Neurol 2006;60:617–618. [PubMed: 16847950]

19. Melrose HL, Kent CB, Taylor JP, et al. A comparative analysis of leucine-rich repeat kinase 2 (Lrrk2) expression in mouse brain and Lewy body disease. Neuroscience 2007;147:1047–1058. [PubMed: 17611037]

20. Higashi S, Biskup S, West AB, et al. Localization of Parkinson's disease-associated LRRK2 in normal and pathological human brain. Brain Res 2007;1155:208–219. [PubMed: 17512502]

21. Giasson BI, Covy JP, Bonini NM, et al. Biochemical and pathological characterization of Lrrk2. Ann Neurol 2006;59:315–322. [PubMed: 16437584]

22. Covy JP, Van Deerlin VM, Giasson BI. Lack of evidence for Lrrk2 in α-synuclein pathological inclusions. Ann Neurol 2006;60:618–619.

23. Paxinou E, Chen Q, Weisse M, et al. Induction of alpha-synuclein aggregation by intracellular nitrative insult. J Neurosci 2001;21:8053–8061. [PubMed: 11588178]

24. Giasson BI, Duda JE, Murray IV, et al. Oxidative damage linked to neurodegeneration by selective alpha-synuclein nitration in synucleinopathy lesions. Science 2000;290:985–989. [PubMed: 11062131]

25. Giasson BI, Jakes R, Goedert M, et al. A panel of epitope-specific antibodies detects protein domains distributed throughout human alpha-synuclein in Lewy bodies of Parkinson's disease. J Neurosci Res 2000;59:528–533. [PubMed: 10679792]

26. Duda JE, Giasson BI, Mabon ME, et al. Novel antibodies to synuclein show abundant striatal pathology in Lewy body diseases. Ann Neurol 2002;52:205–210. [PubMed: 12210791]

27. Baba M, Nakajo S, Tu PH, et al. Aggregation of alpha-synuclein in Lewy bodies of sporadic Parkinson's disease and dementia with Lewy bodies. Am J Pathol 1998;152:879–884. [PubMed: 9546347]

28. Bence NF, Sampat RM, Kopito RR. Impairment of the ubiquitin-proteasome system by protein aggregation. Science 2001;292:1552–1555. [PubMed: 11375494]

29. Burnett B, Li F, Pittman RN. The polyglutamine neurodegenerative protein ataxin-3 binds polyubiquitylated proteins and has ubiquitin protease activity. Hum Mol Genet 2003;12:3195–3205. [PubMed: 14559776]

30. Grant ER, Bacskai BJ, Pleasure DE, et al. N-Methyl-D-aspartate receptors expressed in a nonneuronal cell line mediate subunit-specific increases in free intracellular calcium. J Biol Chem 1997;272:647–656. [PubMed: 8995308]

31. Mazzulli JR, Mishizen AJ, Giasson BI, et al. Cytosolic catechols inhibit alpha-synuclein aggregation and facilitate the formation of intracellular soluble oligomeric intermediates. J Neurosci 2006;26:10068–10078. [PubMed: 17005870]

32. Duda JE, Giasson BI, Gur TL, et al. Immunohistochemical and biochemical studies demonstrate a distinct profile of alpha-synuclein permutations in multiple system atrophy. J Neuropathol Exp Neurol 2000;59:830–841. [PubMed: 11005264]

33. Giasson BI, Covy JP, Bonini NM, et al. Biochemical and pathological characterization of Lrrk2. Ann Neurol 2006;59:315–322. [PubMed: 16437584]

34. Smith WW, Pei Z, Jiang H, et al. Leucine-rich repeat kinase 2 (LRRK2) interacts with parkin, and mutant LRRK2 induces neuronal degeneration. Proc Natl Acad Sci U S A 2005;102:18676–18681. [PubMed: 16352719]

35. Wang L, Xie C, Greggio E, et al. The chaperone activity of heat shock protein 90 is critical for maintaining the stability of leucine-rich repeat kinase 2. J Neurosci 2008;28:3384–3391. [PubMed: 18367605]

36. West AB, Moore DJ, Biskup S, et al. Parkinson's disease-associated mutations in leucine-rich repeat kinase 2 augment kinase activity. Proc Natl Acad Sci U S A 2005;102:16842–16847. [PubMed: 16269541]
37. Hayne C, Tzivion G, Luo Z. Raf-1/MEK/MAPK pathway is necessary for the G_2/M transition induced by nocodazole. J Biol Chem 2000;275:31876–31882. [PubMed: 10884385]
38. Johnston JA, Ward CL, Kopito RR. Aggresomes: A cellular response to misfolded proteins. J Cell Biol 1998;143:1883–1898. [PubMed: 9864362]
39. Garcia-Mata R, Bebok Z, Sorscher EJ, et al. Characterization and dynamics of aggresome formation by a cytosolic GFP-chimera. J Cell Biol 1999;146:1239–1254. [PubMed: 10491388]
40. Waelter S, Boeddrich A, Lurz R, et al. Accumulation of mutant huntingtin fragments in aggresome-like inclusion bodies as a result of insufficient protein degradation. Mol Biol Cell 2001;12:1393–1407. [PubMed: 11359930]
41. Ko HS, Bailey R, Smith WW, et al. CHIP regulates leucine-rich repeat kinase-2 ubiquitination, degradation, and toxicity. Proc Natl Acad Sci U S A 2009;106:2897–2902. [PubMed: 19196961]
42. Lee HJ, Lee SJ. Characterization of cytoplasmic alpha-synuclein aggregates. Fibril formation is tightly linked to the inclusion-forming process in cells. J Biol Chem 2002;277:48976–48983. [PubMed: 12351642]
43. Tanaka M, Kim YM, Lee G, et al. Aggresomes formed by α-synuclein and synphilin-1 are cytoprotective. J Biol Chem 2004;279:4625–4631. [PubMed: 14627698]
44. Ardley HC, Scott GB, Rose SA, et al. UCH-L1 aggresome formation in response to proteasome impairment indicates a role in inclusion formation in Parkinson's disease. J Neurochem 2004;90:379–391. [PubMed: 15228595]
45. Biskup S, Moore DJ, Rea A, et al. Dynamic and redundant regulation of LRRK2 and LRRK1 expression. BMC Neurosci 2007;8:102. [PubMed: 18045479]
46. Santpere G, Ferrer I. LRRK2 and neurodegeneration. Acta Neuropathol 2009;117:227–246. [PubMed: 19142648]
47. Rajput A, Dickson DW, Robinson CA, et al. Parkinsonism, Lrrk2 G2019S, and tau neuropathology. Neurology 2006;67:1506–1508. [PubMed: 17060589]

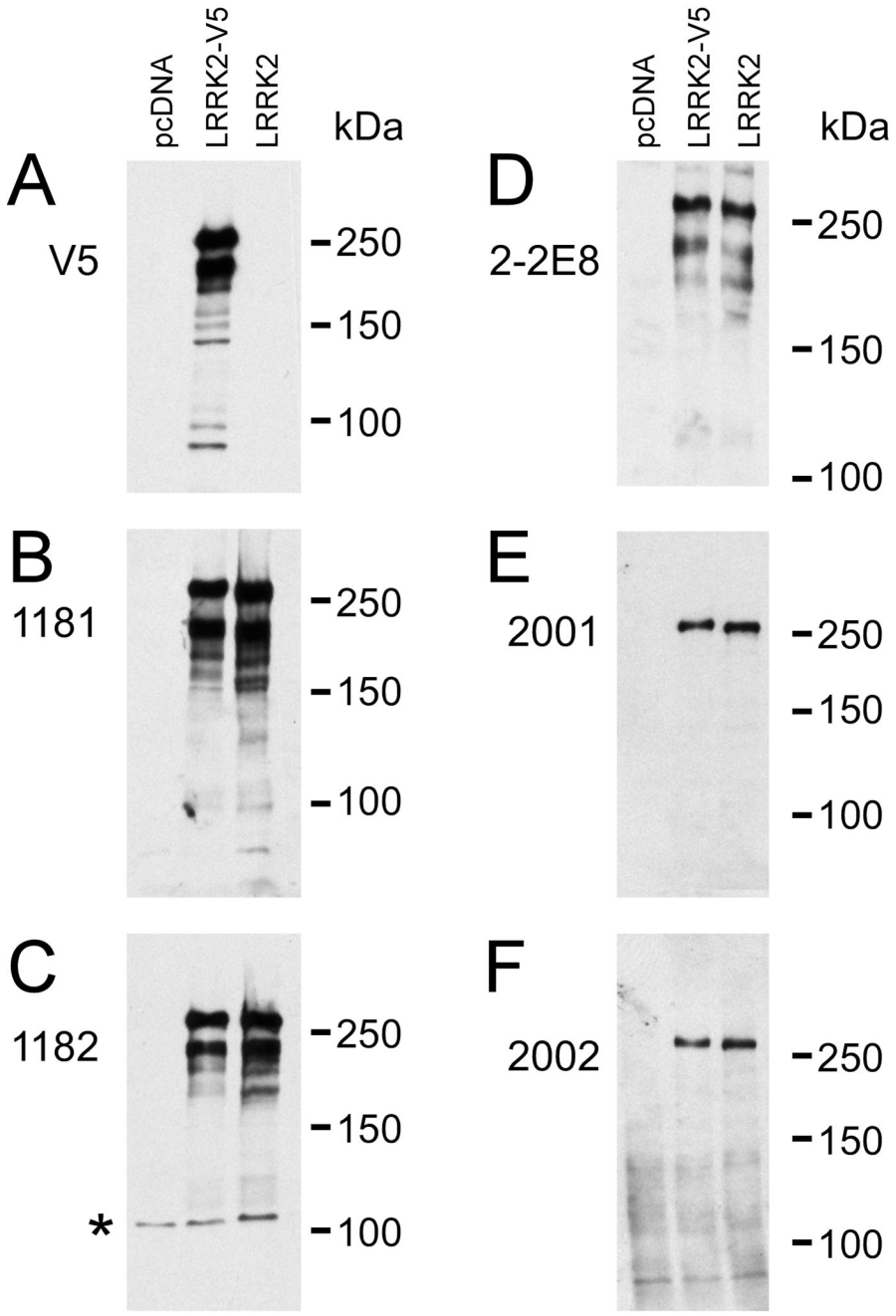

Figure 1.

Specificity of leucine-rich repeat kinase-2 (LRRK2) antibodies. 293t cells were transfected with mock cDNA (pcDNA), LRRK2-V5, or LRRK2. Thirty μg of protein of each lysate was resolved in 6% SDS-polyacrylamide and was analyzed by Western blotting using antibodies (**A**) V5, (**B**) 1181#2, (**C**) 1182#1, (**D**) 2-2E8, (**E**) 2001#1, or (**F**) 2002#2. The numbers indicate the polyclonal bleed presented. Representative immunoblots were overexposed to support the specificity of novel LRRK2 antibodies. *Nonspecific immunoreactivity noted only with 1182#1.

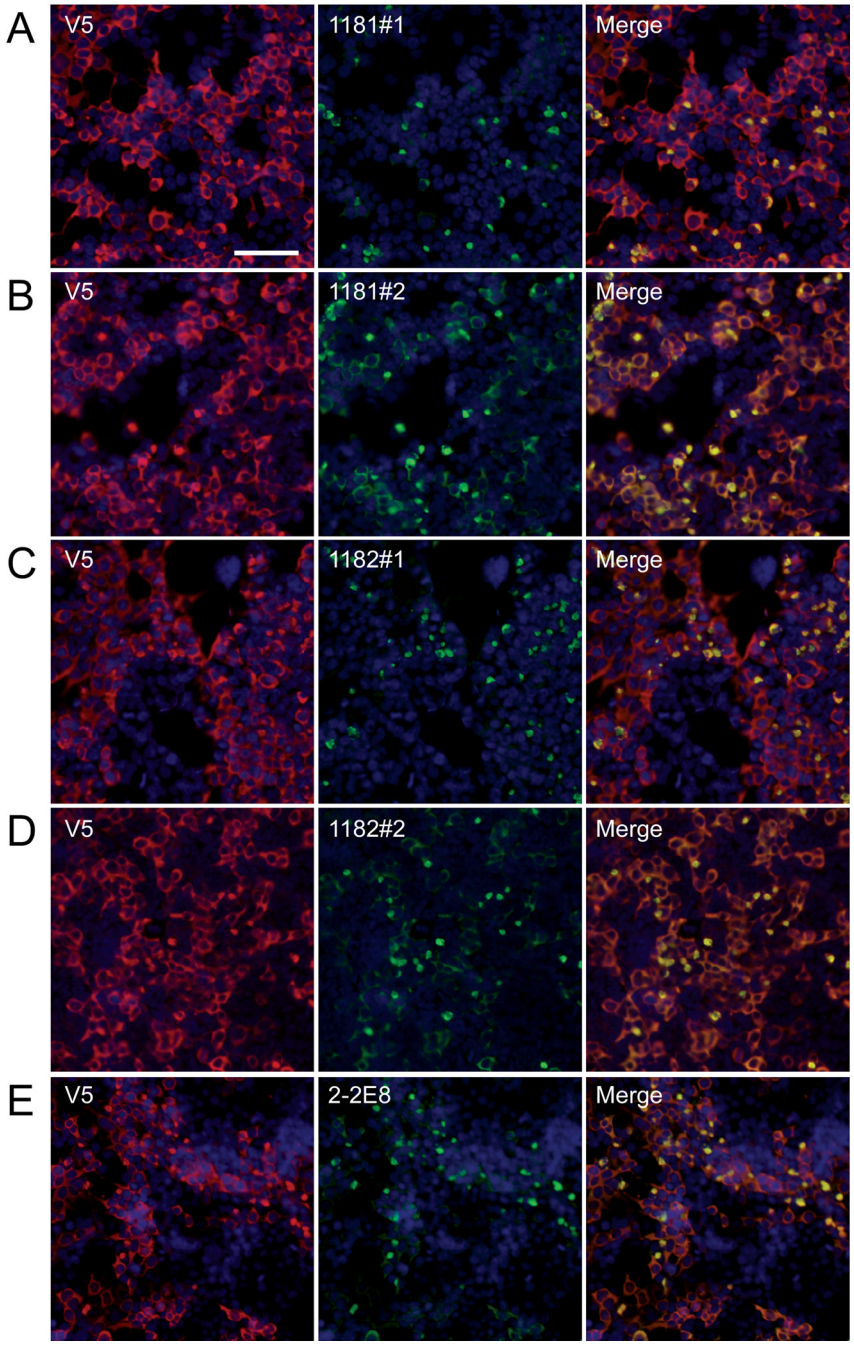

Figure 2.

Immunofluorescence of leucine-rich repeat kinase-2 (LRRK2) in transfected 293t cells. Double immunofluorescence was performed on 293t cells transfected with LRRK2-V5, and immunoreactivity was compared between monoclonal anti-V5 (red, **A–D**) or polyclonal anti-V5 (red, **E**) and LRRK2-specific antibodies (green) 1181#1 (**A**), 1181#2 (**B**), 1182#1 (**C**), 1182#2 (**D**) or 2-2E8 (**E**). Staining with anti-V5 antibody, LRRK2 appeared mostly cytosolic. Some LRRK2-specific antibodies preferentially recognized aggregated forms of LRRK2, observed as perinuclear aggregates in a subpopulation of cells. 1181#1 (**A**) and 1182#1 (**C**) showed greater specificity for the aggregated form, while 1181#2 (**B**) and 1182#2 (**D**)

recognized aggregated and cytosolic forms of LRRK2. The monoclonal LRRK2 antibody 2-2E8 (E) also specifically recognized these aggregates. Bar scale: 100 μm.

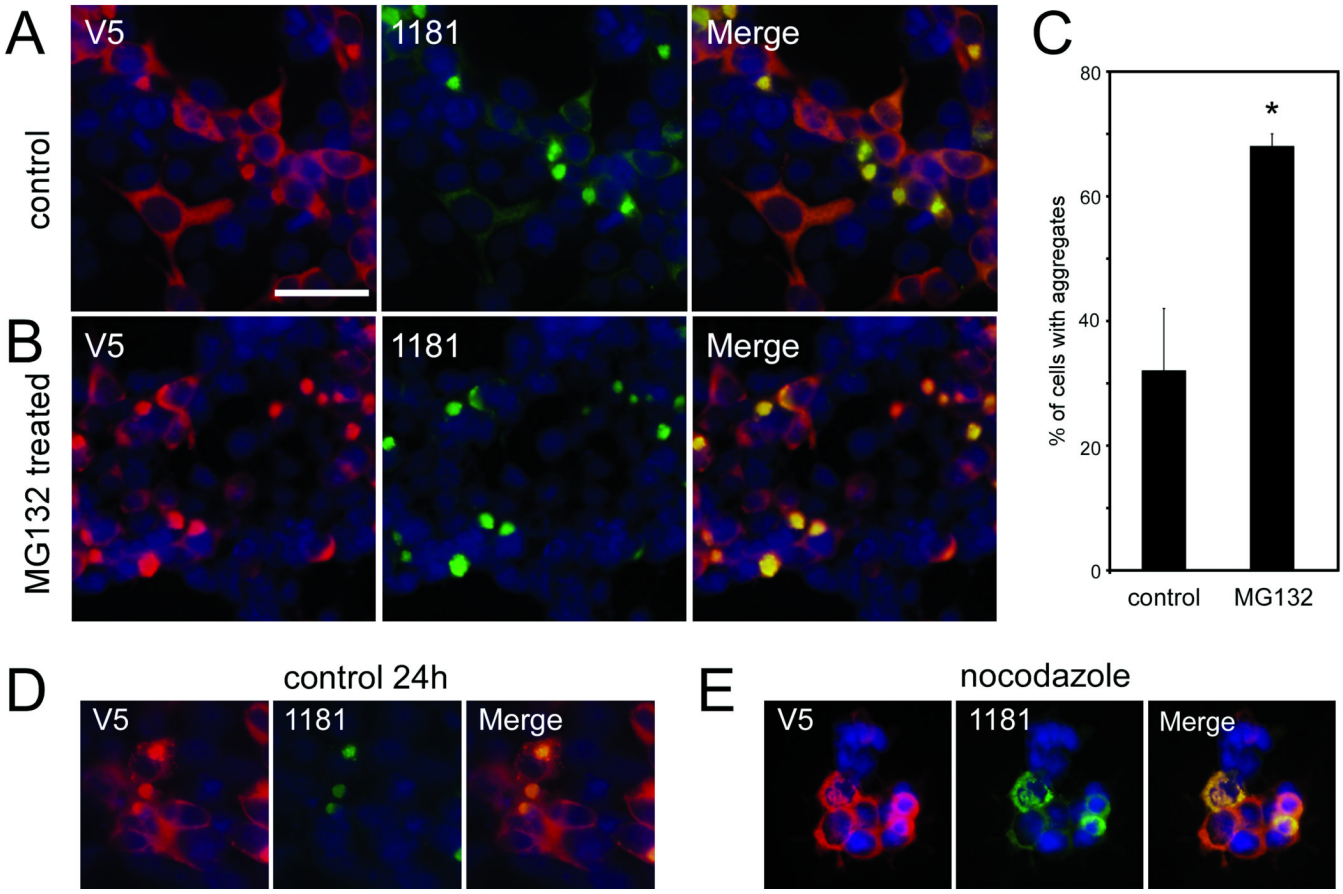

Figure 3.

Characterization of leucine-rich repeat kinase-2 (LRRK2) aggregates in transfected 293t cells. Double immunofluorescence was performed with the monoclonal anti-V5 antibody (red) and 1181#1 (green) in 293t cells transfected with LRRK2-V5. 32 hours after transfection, cells were treated with vehicle (**A**) or MG132 (10 μM) (**B**) for 16 hours before fixation. (**C**) Quantitative assessment of cells containing large aggregates, as determined by independent cell counts, comparing control to MG132 treatment. Data represent average ± SD (*, $p = 0.004$; $n = 3$). (**D**) Transfected 293t cells begin forming aggregates within 24 hours after transfection, and (**E**) perinuclear aggregate formation is blocked by treatment with nocodazole from 12 hours after transfection until fixation at 24 hours post-transfection. Images are representative of 3 independent experiments. Bar scale: 50 μm.

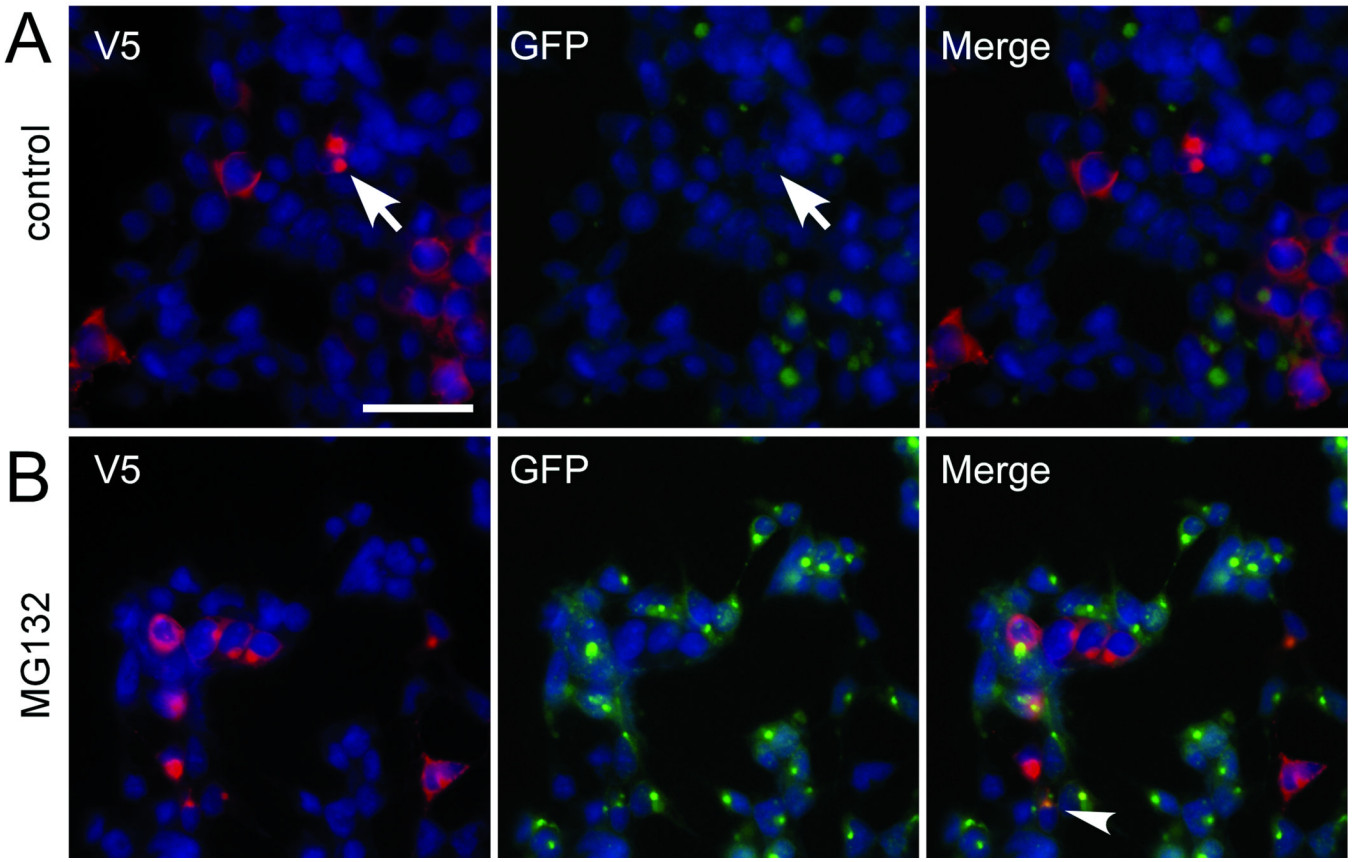

Figure 4.

Leucine-rich repeat kinase-2 (LRRK2) expression or aggregate formation does not change levels of GFP-u. LRRK2-V5 was used to transfect cells that stably express a short-lived GFP that is degraded by the proteasome (GFP-u). Double immunofluorescence was performed between a monoclonal anti-V5 antibody (red) and GFP (green). Under basal conditions (**A**), cells with aggregates (arrows) do not increase GFP fluorescence. (**B**) MG132 treatment (10 μM, 16 hours) increased GFP fluorescence of all cells. GFP colocalized with LRRK2 aggregates in some cells (arrowhead). Images are representative of 3 independent experiments. Bar scale: 50 μm.

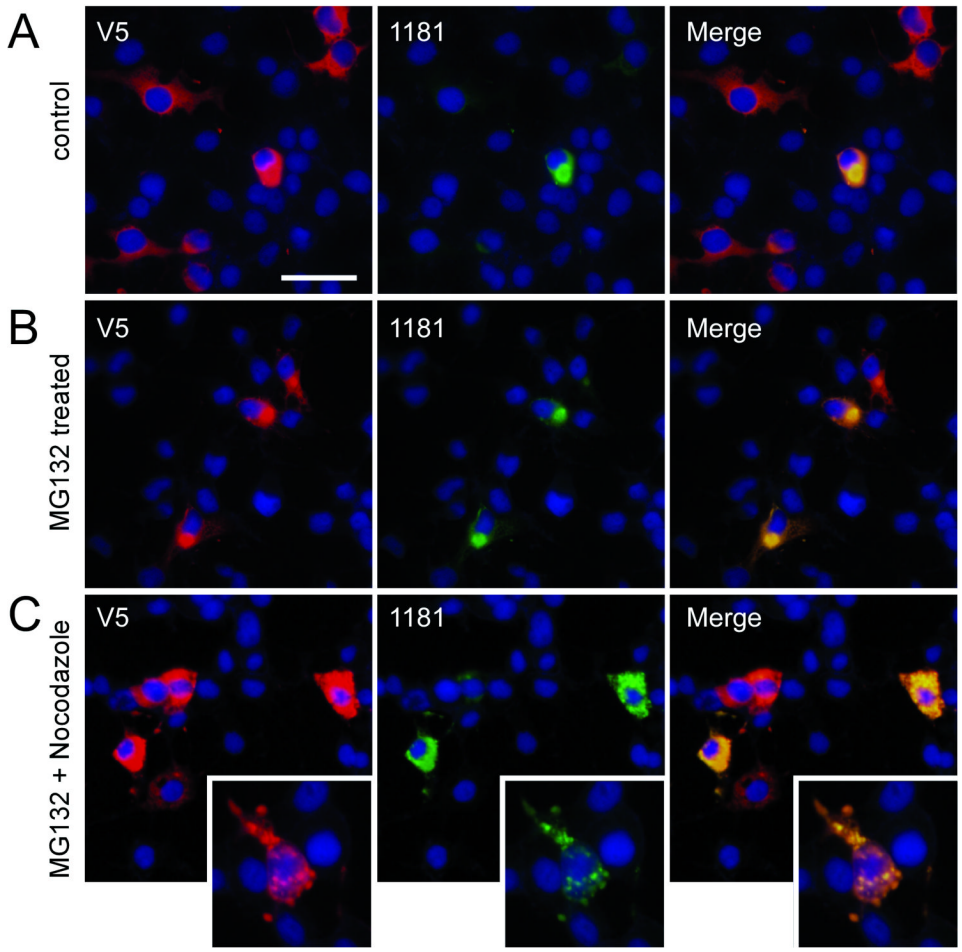

Figure 5.

Leucine-rich repeat kinase-2 (LRRK2) aggregates in transfected COS-7 cells. Double immunofluorescence was performed with a monoclonal anti-V5 antibody (red) and 1181#1 (green) in COS-7 transfected with LRRK2-V5. (**A**) Rare large aggregates were observed under basal conditions at 48 hours post-transfection. (**B**) Sixteen hours of MG132 (10 μm) treatment induced aggregate formation. (**C**) MG132 treatment with concomitant nocodazole prevented the formation of large, perinuclear aggregates. Small aggregates throughout the cytosol were noted with nocodazole treatment (inset). Images are representative of 3 independent experiments. Bar scale: 50 μm; inset 25 μm.

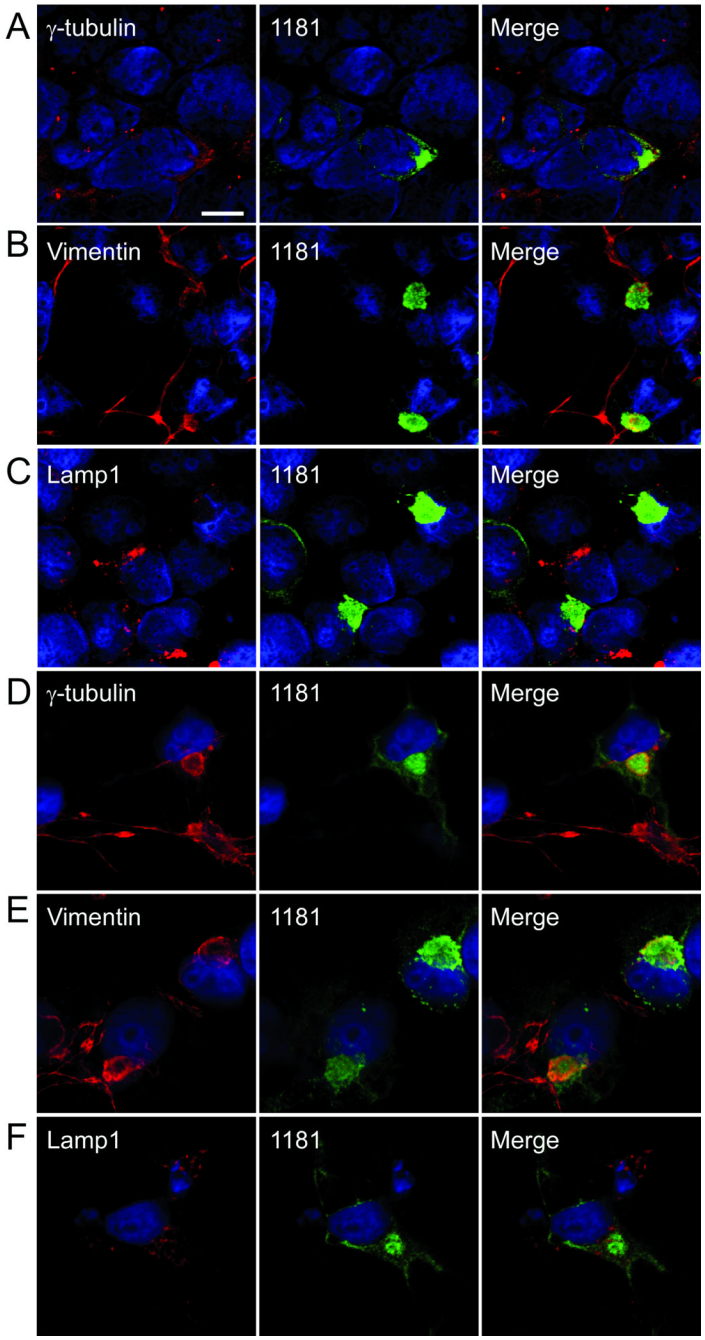

Figure 6.

Confocal microscopy showing colocalization of LRRK2 with markers of aggresome formation. (**A–C**) 293t cells were transfected with LRRK2, and (**D–F**) COS-7 cells were transfected with LRRK2 and treated with MG132 (10 μM, 16 hours) and then double immunofluorescence was performed between aggresome markers anti-γ-tubulin (**A, D**), antivimentin **(B, E**), or anti-lamp1 (**C, F**) and 1181#1. Colocalization was observed for both γ-tubulin and vimentin. Some lamp1 immunofluorescence was noted around the LRRK2 aggregate. All images provided are of a single Z-plane of <0.7 μm. Bar scale: 10 μm.

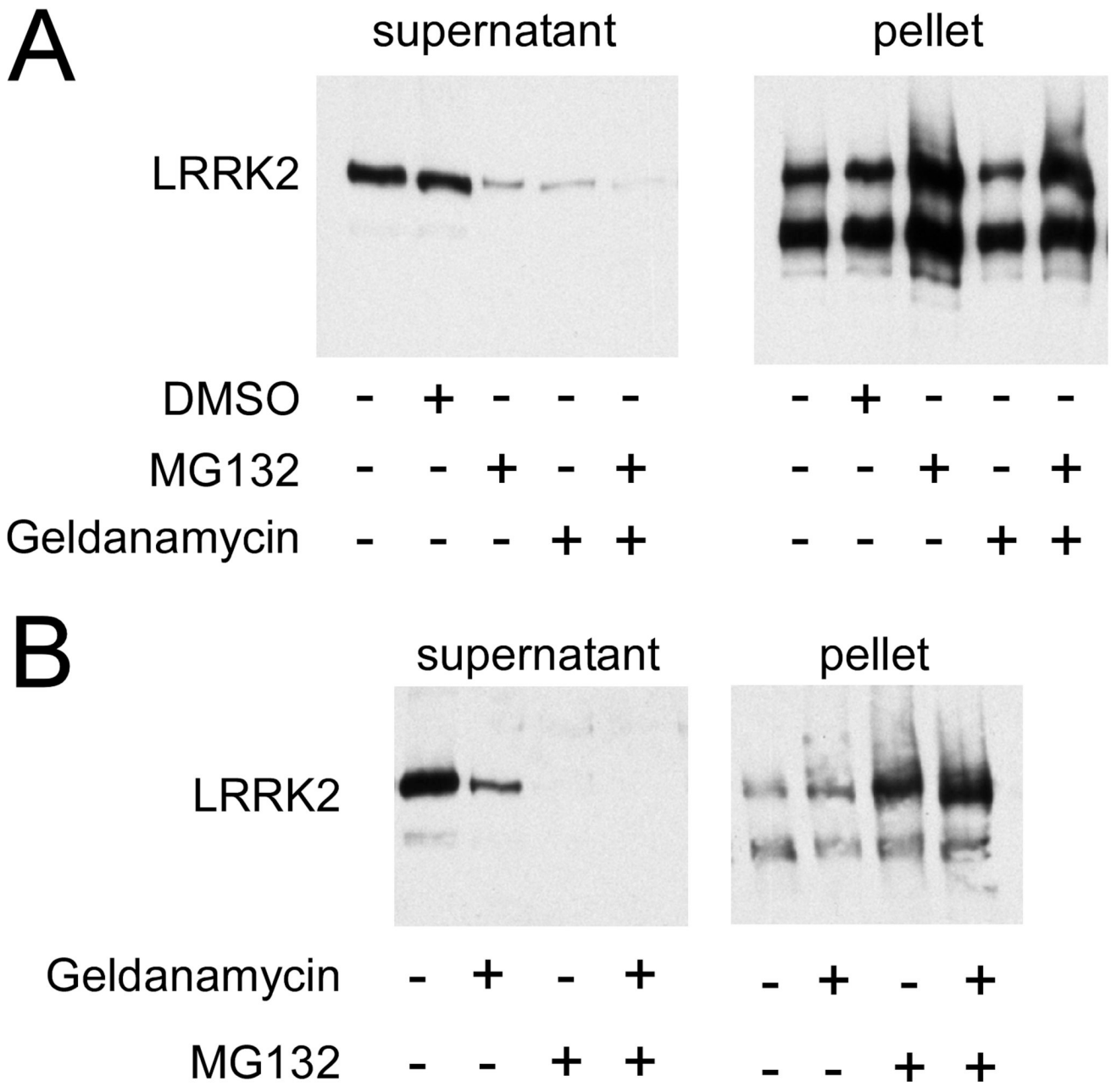

Figure 7.

Biochemical cellular fractionation of LRRK2 expressed in transfected 293t cells. 293t cells were transfected with LRRK2-V5 and fractionated based on solubility. Western blot analysis was performed with a monoclonal anti-V5 antibody. (**A**) Cells were treated 32 hours after transfection with vehicle (DMSO), MG132 (10 μM) and/ or geldanamycin (500 nM), and then harvested after 16 hours of treatment. Control cells resulted in 61% ± 16% (SD) pelleted LRRK2, which was increased to 95% ± 7% (SD) pelleted with MG132 treatment ($p = 0.001$, $n = 5$). Geldanamycin treatment resulted in 86% ± 17% (SD) insoluble LRRK2. This change in percent resulted from a loss of LRRK2 in the supernatant ($p = 0.04$, $n = 3$) and not a redistribution from the soluble to pellet fraction. Concomitant treatment of MG132 and geldanamycin resulted in 93% ± 9% of LRRK2 in the pellet, similar to that of MG132 treatment

alone. (**B**) Twelve hours after transfection, cells were challenged with drugs for an additional 12 hours prior to experimentation. Geldanamycin treatment reduced the amount of LRRK2 in the supernatant, but did not alter the LRRK2 in the pellet. MG132 redistributed LRRK2 into the pellet, independent of geldanamycin treatment (n = 2).

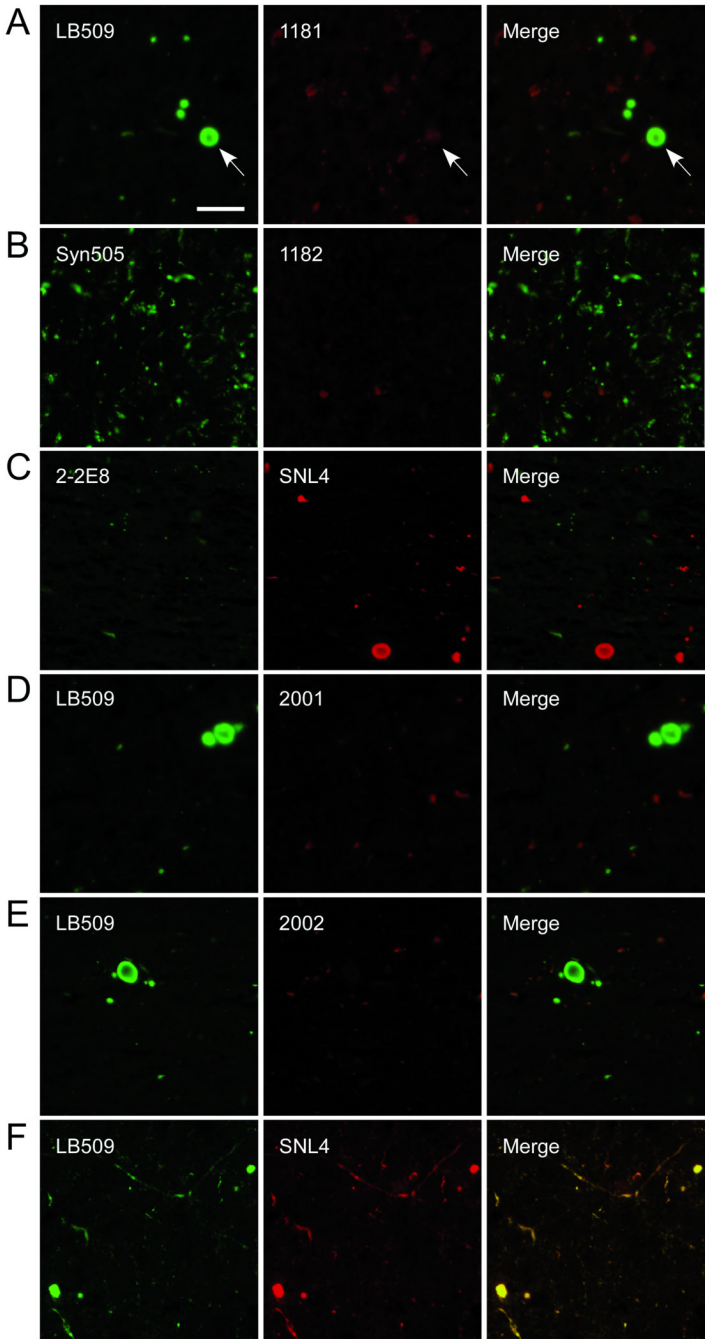

Figure 8.

Double immunofluorescence of human brain sections containing pathological α-synuclein (α-syn) inclusions with anti-LRRK2 and anti-α-syn antibodies. Tissue sections from the substantia nigra (**A, C–F**) from patients with diffuse Lewy body disease (**C, E, F**) or Lewy body variant of Alzheimer disease (**A, D**) and cingulate gyrus from a patient with Parkinson disease (**B**) were examined by double immunofluorescence with anti-LRRK2-specific antibodies (1181#1, 1182#1, 2-2E8, 2001#1, 2002#2) and α-syn-specific antibodies (LB509, Syn505, or SNL4). Antibody 1181#1 (**A**, red) showed faint immunoreactivity for some rare α-syn-positive Lewy bodies (LB) (arrow) but this immunoreactivity did not exhibit typical LB morphology. 1182#1 (**B**, red), 2-2E8 (**C**, green), 2001 (**D**, red), and 2002 (**E**, red) demonstrated no immunoreactivity

for LBs, Lewy neurites or neuroaxonal spheroids. (**F**) Control showing that the mouse monoclonal anti-α-syn antibodies LB509 (green) and rabbit polyclonal anti-α-syn SNL4 (red) had identical immunoreactivities. Bar scale: 50 μm.

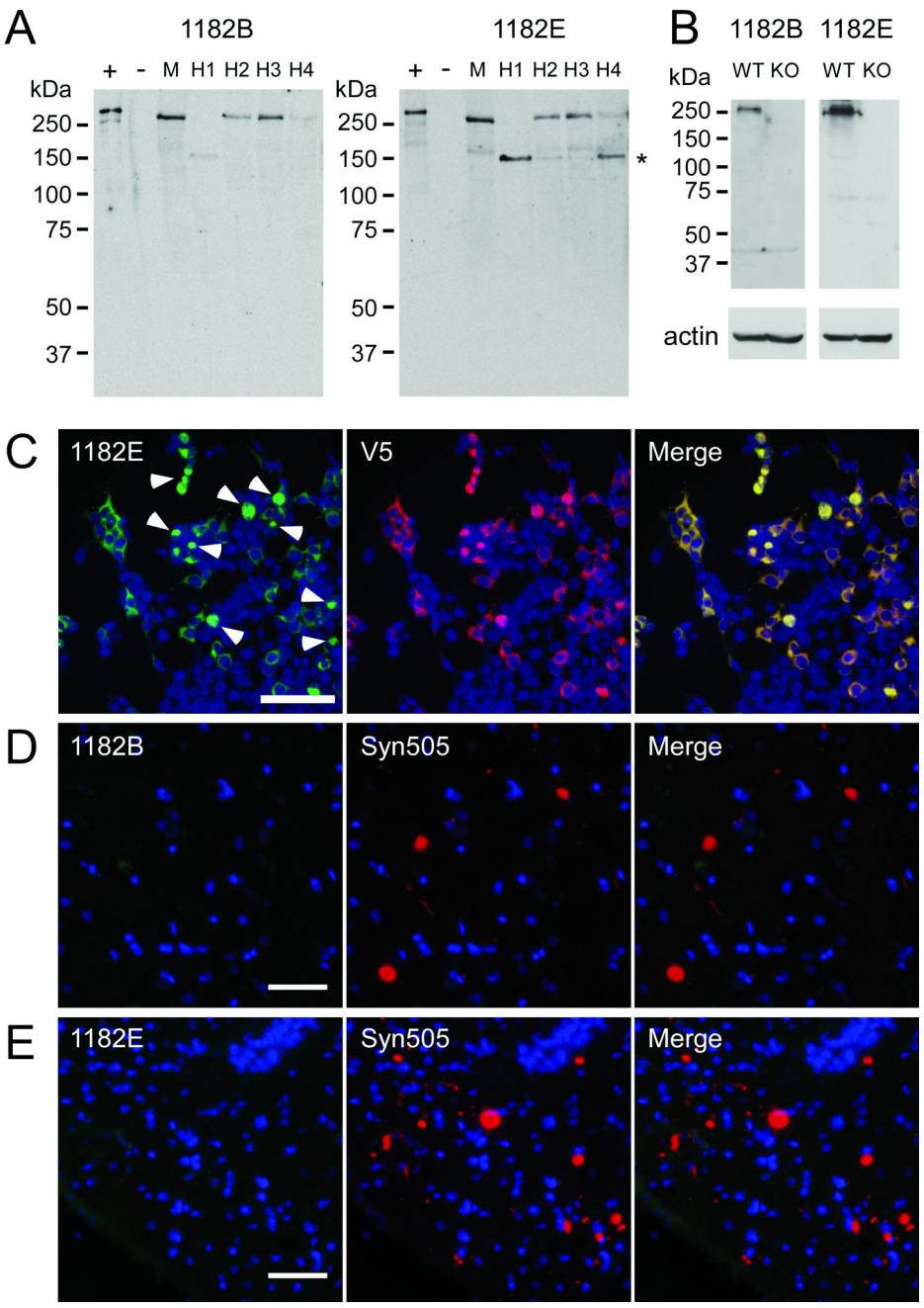

Figure 9.

Characterization of affinity-purified LRRK2 antibody. Antibody 1182 was affinity purified using peptides B and E resulting in affinity-purified antibodies termed 1182B and 1182E. (**A**) Western blot analysis demonstrating the ability of affinity purified antibodies 1182B and 1182E to detect endogenous LRRK2 in soluble extracts from cerebral cortex of a normal mouse (M) and 4 different humans (H1-4). Lanes + and − were loaded with 0.5 μg of soluble lysates from 293t cells transfected with LRRK2-V5 or mock cDNA (pcDNA), respectively. Lanes M and H1-4 were loaded with 100 μg of protein extracts. The mobility of molecular mass markers is indicated on the left. The major LRRK2 breakdown product is indicated with an asterisk (*). (**B**) Western blot analysis of wild-type (WT) and LRRK2 knockout (KO) mice with affinity

purified LRRK2-antibodies, 1182B and 1182E. A specific band of the molecular weight of LRRK2 was recognized only in WT mice. Actin immunoreactivity is shown as a loading control. (**C**) Double immunofluorescence staining with antibody 1182E and anti-V5 antibody in 293t cells transfected with LRRK2-V5. Antibody 1182E immunolabeled both cytosolic and aggregated (arrowheads) LRRK2. (**D**) Double immunofluorescence with antibodies 1182B and Syn505 on cingulate cortex of a patient with diffuse Lewy body disease. (**E**) Double immunofluorescence with antibodies 1182E and Syn505 on substantia nigra of a patient with the LRRK2 G2019S mutation and Parkinson Disease. The affinity-purified anti-LRRK2 antibodies did not label any Lewy bodies or Lewy neurites. Bar scales: C = 100 μm; D, E = 50 μm.

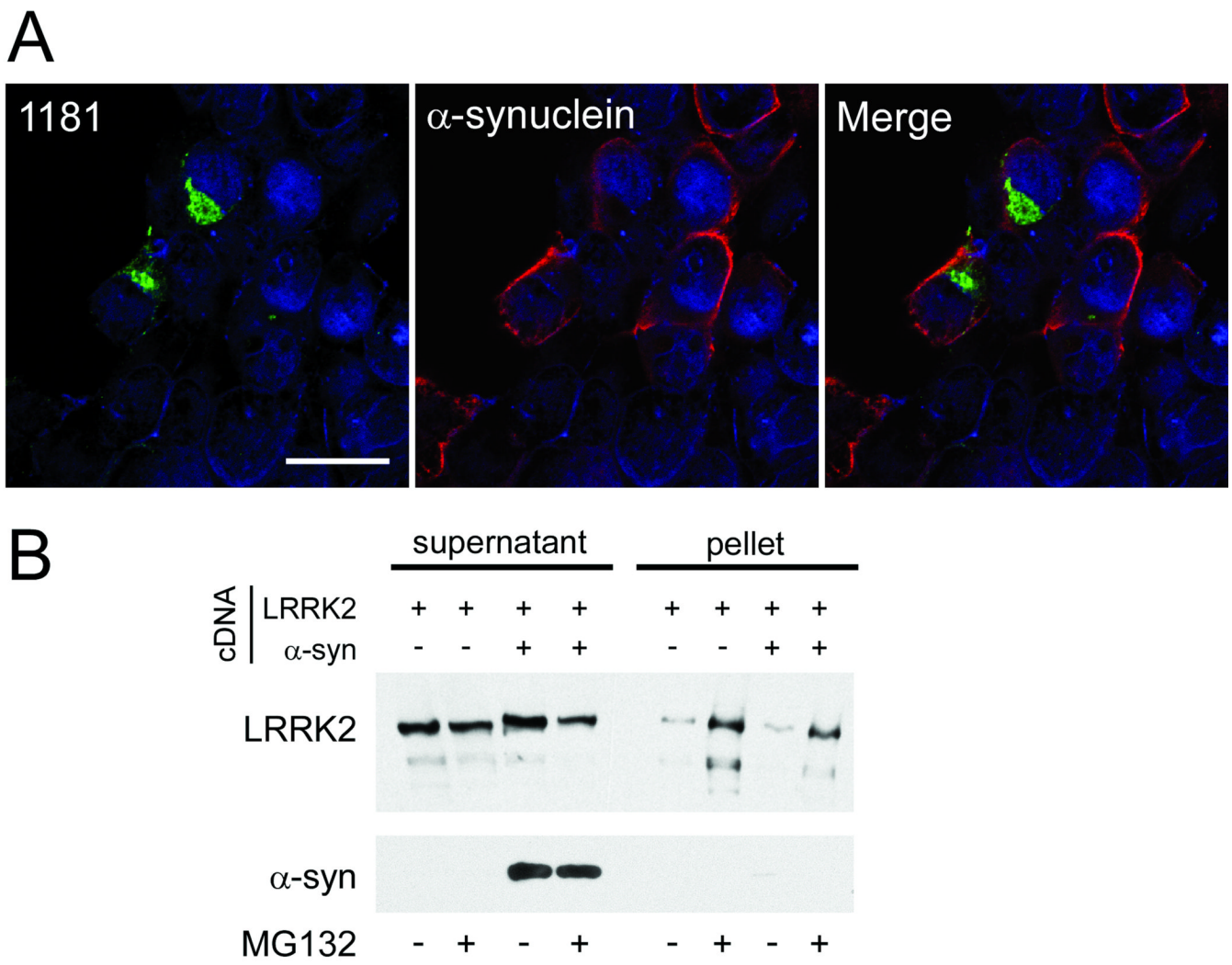

Figure 10.

LRRK2 aggresome formation does not alter the localization of α-synuclein (α-syn). (**A**) Confocal microscopy of 293t cells co-transfected with LRRK2-V5 and pcDNA3.1/α-syn and treated with MG132 (10 μM, 16 hours). LRRK2 (1181#1; green) formed aggresomes, but α-syn (antibody Syn211, red) remained cytosolic. The image is a single Z-plane of <0.7 μm. Bar scale: 20 μm. (**B**) 293t cells were transfected with LRRK2-V5 and mock cDNA or pcDNA3.1/α- syn and then treated with MG132. Biochemical cellular fractionation and immunoblotting were performed with anti-V5 or Syn211. LRRK2 redistributed to the insoluble fraction with MG132 treatment, both with and without α-syn co-transfection. α-Syn did not change solubility with MG132 treatment. Data are representative of 3 independent experiments.

Table

Diagnoses and Demographics of Cases Examined by Immunohistochemistry

Case No.	Diagnosis	Age (years)	Sex	Postmortem Interval (hours)
1	PD (A53T)	49	M	NA
2	NBIA-1	28	M	6
3	PD (GS)	67	M	7
4	PD (GS)	88	M	15
5	PD (GS)	78	M	8
6	LBVAD	82	M	12
7	LBVAD	66	M	11
8	PD	81	M	5
9	PD (LP)	81	M	13
10	LBVAD	90	M	15
11	PD (RM)	92	M	6
12	PD	78	M	16
13	PD	87	M	8
14	MSA	73	M	8
15	DLB	75	M	16
16	PD (A53T)	57	M	3
17	LBVAD	74	F	18
18	PD	74	M	7
19	MSA	57	M	11
20	MSA	75	M	19
21	PD	76	M	11
22	LBVAD	65	F	3
23	LBVAD	62	M	11
24	MSA	63	M	19
25	DLB	79	M	2
26	DLB	79	F	6
27	PD	86	F	21
28	MSA	64	M	15

Abbreviations: PD, Parkinson disease; A53T, familial mutation in α-synuclein A53T; (GS), LRRK2 mutation G2109S; (LP), LRRK2 mutation L1165P; (RM), LRRK2 mutation R793M; NBIA-1, neurodegeneration with brain iron accumulation 1; LBVAD, Lewy body variant of Alzheimer disease; MSA, multiple systems atrophy; DLB, dementia with Lewy bodies. NA, not available. M, male; F, female.